Report

Cell Reports

Cortical Interneurons Differentially Shape Frequency Tuning following Adaptation

Graphical Abstract

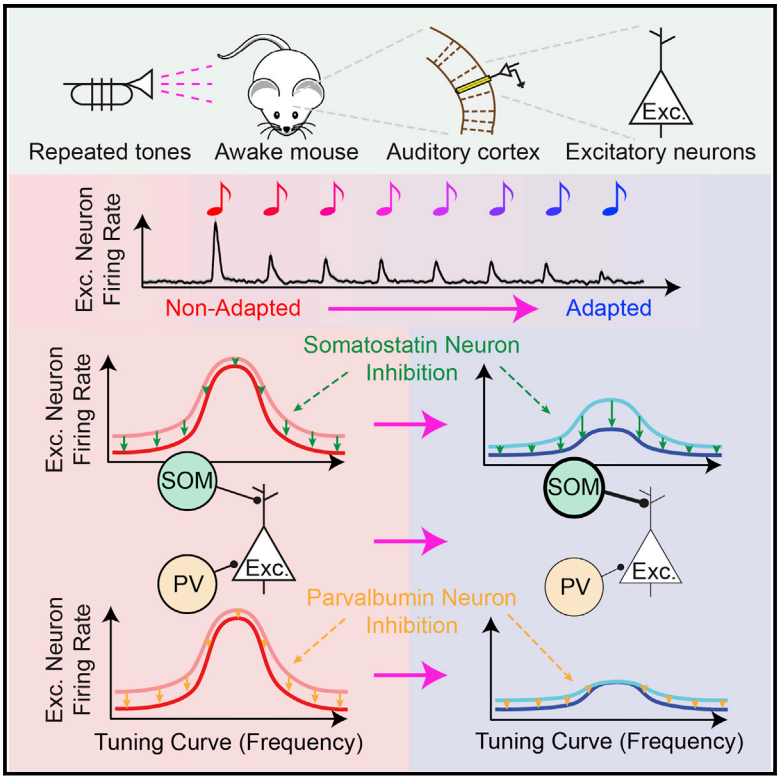

Authors

Ryan G. Natan, Winnie Rao, Maria N. Geffen

Correspondence

mgeffen@med.upenn.edu

In Brief

Natan et al. describe how a specific component in the neural circuitry in a key auditory part of the brain helps the auditory system tease apart complex sounds. This happens through adaptation of neuronal responses to temporally repeated sounds.

Highlights

- Inhibition facilitates cortical adaptation to repeated tones
- Different inhibitory interneuron function diverges
- Somatostatin-positive interneurons support adaptation to temporal context
- Neurons adapt to temporal repetition to efficiently process sound

Natan et al., 2017, Cell Reports *21*, 878–890
October 24, 2017
https://doi.org/10.1016/j.celrep.2017.10.012

OPEN ACCESS
CellPress

Cell Reports
Report

Cortical Interneurons Differentially Shape Frequency Tuning following Adaptation

Ryan G. Natan,[1,2] Winnie Rao,[1] and Maria N. Geffen[1,3,*]
[1]Department of Otorhinolaryngology: HNS and Department of Neuroscience, University of Pennsylvania, Philadelphia, PA, USA
[2]Present address: Janelia Campus, Howard Hughes Medical Institute, Ashburn, VA, USA
[3]Lead Contact
*Correspondence: mgeffen@med.upenn.edu
https://doi.org/10.1016/j.celrep.2017.10.012

SUMMARY

Neuronal stimulus selectivity is shaped by feedforward and recurrent excitatory-inhibitory interactions. In the auditory cortex (AC), parvalbumin- (PV) and somatostatin-positive (SOM) inhibitory interneurons differentially modulate frequency-dependent responses of excitatory neurons. Responsiveness of neurons in the AC to sound is also dependent on stimulus history. We found that the inhibitory effects of SOMs and PVs diverged as a function of adaptation to temporal repetition of tones. Prior to adaptation, suppressing either SOM or PV inhibition drove both increases and decreases in excitatory spiking activity. After adaptation, suppressing SOM activity caused predominantly disinhibitory effects, whereas suppressing PV activity still evoked bi-directional changes. SOM, but not PV-driven inhibition, dynamically modulated frequency tuning with adaptation. Unlike PV-driven inhibition, SOM-driven inhibition elicited gain-like increases in frequency tuning reflective of adaptation. Our findings suggest that distinct cortical interneurons differentially shape tuning to sensory stimuli across the neuronal receptive field, altering frequency selectivity of excitatory neurons during adaptation.

INTRODUCTION

Neurons throughout the sensory pathway are tuned to specific aspects of stimuli, such as position and edge orientation in the visual cortex or frequency and its modulation in the auditory cortex. This selectivity is thought to determine behavioral and perceptual discrimination in the natural world. Excitatory neuron selectivity is shaped by both feedback and recurrent networks, including excitatory-inhibitory interactions. These interactions are complex: inhibitory neurons exhibit remarkable diversity in their morphology and physiological properties, as well as the complexity in connectivity patterns, targeting excitatory as well as other inhibitory neurons (Isaacson and Scanziani, 2011). The two most common classes of inhibitory neuron, parvalbumin- (PV) and somatostatin- (SOM) positive interneurons, are thought to differentially shape excitatory neuronal responses. PVs predominantly target the cell bodies of excitatory neurons (Wang et al., 2002), whereas the majority of SOMs target the distal dendrites of excitatory neurons (Ma et al., 2006). In the auditory cortex, recent studies found that PVs and SOMs contribute to tone frequency representation and behavioral selectivity (Aizenberg et al., 2015; Li et al., 2014; Natan et al., 2015; Seybold et al., 2015).

Whereas the majority of these studies relied on static stimuli presented in isolation, auditory processing is inherently dynamic and neurons throughout the auditory pathway, including the auditory cortex, adjust their response properties to sounds depending on the stimulus statistics. The most prevalent form of such changes occurs through adaptation. By reducing the signaling strength in response to commonly encountered stimuli, neuronal populations enhance sensitivity to changes in those stimuli (Solomon and Kohn, 2014). This process is thought to increase information transmission and computational efficiency of neuronal networks (Schwartz and Simoncelli, 2001). Adaptation is thought to rely largely on feedforward synaptic depression that drives gain adaptation (Abbott et al., 1997). However, it can also be produced through recurrent network dynamics, and as shown in other modalities, recurrent inhibition can contribute to neuronal response dynamics over variable timescales (Geffen et al., 2007; Solomon and Kohn, 2014). Neurons in the auditory cortex exhibit selectivity to sound that is highly context dependent (Dahmen et al., 2010; Ulanovsky et al., 2003): in particular, neurons throughout the auditory pathway, including those in the cortex, exhibit adapting responses depending on the temporal regularity of sounds (Ulanovsky et al., 2003). Recently, we and others showed that PVs and SOMs both provide enhanced inhibition in the adapted regime (Chen et al., 2015; Natan et al., 2015). However, we currently lack an understanding of whether the differential action of PVs and SOMs generalizes to adaptation in all forms and how PVs and SOMs transform tone-frequency representation in the auditory cortex before and after adaptation. Our goal was to arrive at an understanding of whether interneurons provide excitatory neurons with static or dynamic modulation across their frequency tuning curve and over time.

To investigate how PVs and SOMs differentially shape the tuning curve of excitatory neurons before and after adaptation, we presented repeated tones at different frequencies to an awake, head-fixed mouse and recorded neuronal activity while optogenetically inactivating either PVs or SOMs on a subset of trials (Figures 1 and 2).

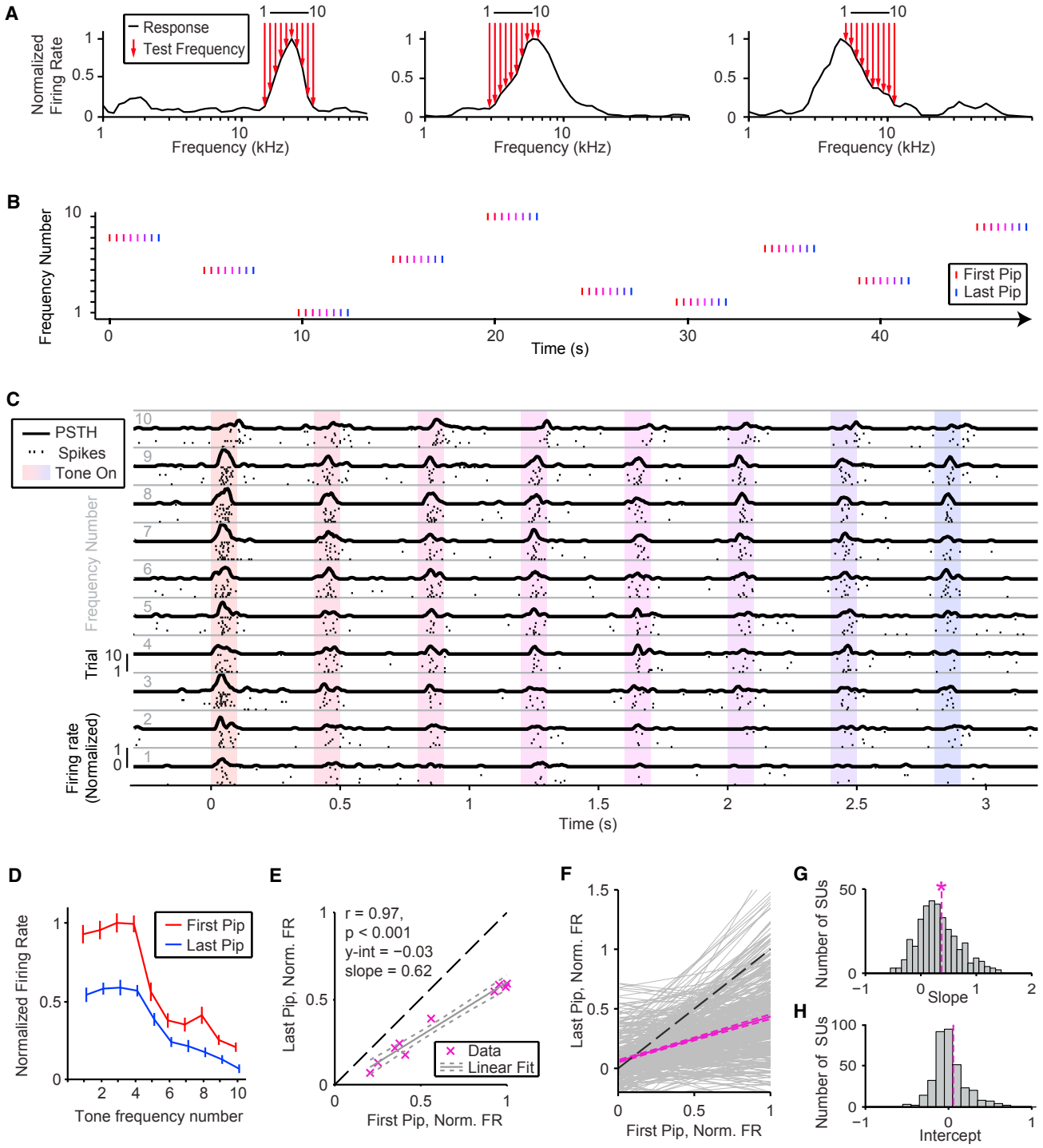

Figure 1. Adaptation Scales Responses across Tuning Curve

(A) Tuning curves (black) of three neurons and the 10 tones (red) selected to construct the tone train stimulus set.

(B) Each tone train is composed of 8 tone pips of a single frequency and is separated by 1.6-s inter-trial interval. Color illustrates the tone's progression from novel (red) to standard (blue).

(C) Rasters and PSTHs depict a single neuron's response to tone trains (shaded areas, color as in B) of each frequency.

(D) Mean firing rate of the same neuron in (C) in response to first (red) and last (blue) tone pip of each train across selected frequencies. Here and below error bars represent SE.

(legend continued on next page)

RESULTS

Cortical Neurons Exhibit Adaptation to the Stimulus

We measured neuronal frequency response functions in awake, head-fixed mice and then presented repeated tones across 10 frequencies that covered a range of the neuronal frequency response function, evoking different response amplitudes (Figures 1A and 1B). Neurons responded to repeated tones with an initially strong response, which gradually reduced over tone pip repeats (Figure 1C), exhibiting adaptation.

Temporal Adaptation Divisively Scales Neuronal Responses across the Tuning Curve

We first assayed the structure of adaptation to repeated tones across neuronal tuning curves by measuring the mean spiking response to the first and last tone pip at each of 10 frequencies (Figure 1D). For each neuron, plotting the first tone response to each test frequency on the x-axis sorts the neuron's tuned responses from preferred to non-preferred frequency (Figure 1E). In an adapting neuron, a linear fit of the first-versus-last tone-evoked responses across frequencies exhibiting a non-significant y-intercept, and a significant slope <1 would indicate divisive scaling. For all neurons that exhibited any optogenetic modulation during tone-evoked activity, in either SOM-Arch (n = 184 neurons from 6 mice over 4 sessions each) or PV-Arch (n = 169 neurons from 5 mice over 4 sessions each) mice, the average responses exhibited divisive scaling after adaptation (slope <1 and intercept not significantly different from 0; Figures 1F–1H). These findings overall support a *divisive adaptation* model for temporal adaptation to repeated sounds.

Optogenetic Manipulation of PV and SOM Activity

Divisive adaptation requires that the response attenuation across the tuning curve be frequency specific, i.e., spiking is reduced more strongly in the center as compared to the tuning sidebands (Figure 2A). Following on our recent finding for differential control of stimulus-specific SSA by PVs and SOMs, we hypothesized that these neurons may play distinct roles in temporal adaptation: PVs would provide uniform suppression in both adapted and non-adapted states, whereas SOM suppression would be selective for the adapted state and be greater for frequencies in the center of the receptive field and weaker for receptive field sidebands (Figures 2B–2D).

Suppressing SOMs or PVs in auditory cortex via Cre-driven expression of archaerhodopsin (Figures 2E–2G) modulated spontaneous spiking in many neurons, as expected. Neuronal populations in SOM-Cre and PV-Cre mice exhibited increased (42% and 74%), decreased (5% and 9%), or unchanged (53% and 17%) spontaneous firing rates, respectively (Figures 2H and 2I). Putative Cre-expressing interneurons, exhibiting significantly suppressed firing rates, were excluded from further analysis of the putative pyramidal neuron population.

Suppression differentially affected baseline and tone-evoked activity. For a representative neuron, the spontaneous firing rate was only slightly increased (Figure 2J) either before or after the tone train during light-on trials, whereas the responses to the first and the last tone were significantly increased.

The Effects of SOM, but Not PV Suppression, Differ between Adapted and Non-adapted Regimes

To test how SOM and PV activity impacted tuned responses relative to adaptation, we selected a subset of putative excitatory neurons that individually exhibited frequency tuning both before and after adaptation, i.e., each neuron's first versus last tone response profile (as in Figure 1E) exhibited slope greater than 1 and intercept was not significantly different from 0 (Figures S1A and S1B). These subsets of neurons were well suited to represent the range of frequency-dependent responses because stimulus test frequencies spanned each neuron's frequency response function from near best frequency (within 2/5ths of an octave) to below the half-maximum response strength. We first confirmed that adaptation was similar in neurons from SOM-Cre (n = 55) and PV-Cre (n = 23) groups: there was no significant difference in the slope ($p = 0.211$; $t(76) = 1.26$) or intercept ($p = 0.714$; $t(76) = 0.37$; Figures S1C and S1D), and the population mean responses reflected divisive adaptation (as in Figure 1F). As expected, each group's population mean neuronal response to tone trains exhibited adaptation (Figures 3A and 3B), responding to first tone pips more strongly than to last tone pips. Typically, neuronal firing rates were disinhibited when either PVs or SOMs were suppressed before or after the tone train.

Suppressing SOM neurons drove differential disinhibition, pecific to the adapted state. SOM suppression had no overall effect on responses to the first tone pips over the recorded population ($p = 0.985$; $t(54) = -0.02$) but significantly disinhibited responses to the last tone pips ($p = 0.001$; $t(54) = 3.40$). Change in neuronal responses due to SOM inhibition significantly increased from the first to last tone pip ($p = 0.007$; $t(54) = 2.79$; Figures 3C and 3D). The time course of the difference in the tone-evoked responses during light-on and light-off conditions differed significantly between responses to the first and last tone pips, further illustrating that adaptation shifted the effect of SOM suppression toward disinhibition. These findings suggest the SOMs provide tone-evoked inhibition, which increases in the adapted regime.

In contrast, whereas suppressing PVs drove a significant increase in spontaneous activity, PV suppression resulted in no significant change in the tone-evoked response over the neuronal population for either the first ($p = 0.701$; $t(22) = -0.39$) or last tones ($p = 0.688$; $t(22) = 0.41$; Figures 3E and 3F). Suppressing PVs drove a similar amount of suppression and activation, resulting in a non-significant difference across the population and no significant difference between the adapted and non-adapted responses ($p = 0.138$; $t(22) = 1.54$). These results suggest that PVs provide equal amount of excitation and inhibition to the excitatory neurons in either adapted or non-adapted state.

(E) Mean firing rate of the same neuron in response to the first versus last tone pip across the selected frequencies (purple). Black, unity line; grey, linear fit (solid) and fit error (dashed).
(F) Linear fit to first versus last pip firing rate responses for each neuron (gray) and population mean (purple) pooled across SOM- and PV-Cre.
(G and H) Slope (G) and intercept (H) of the linear fit for all neurons. Asterisk, significantly different than 1 (G) or 0 (H). Dashed line, population mean.

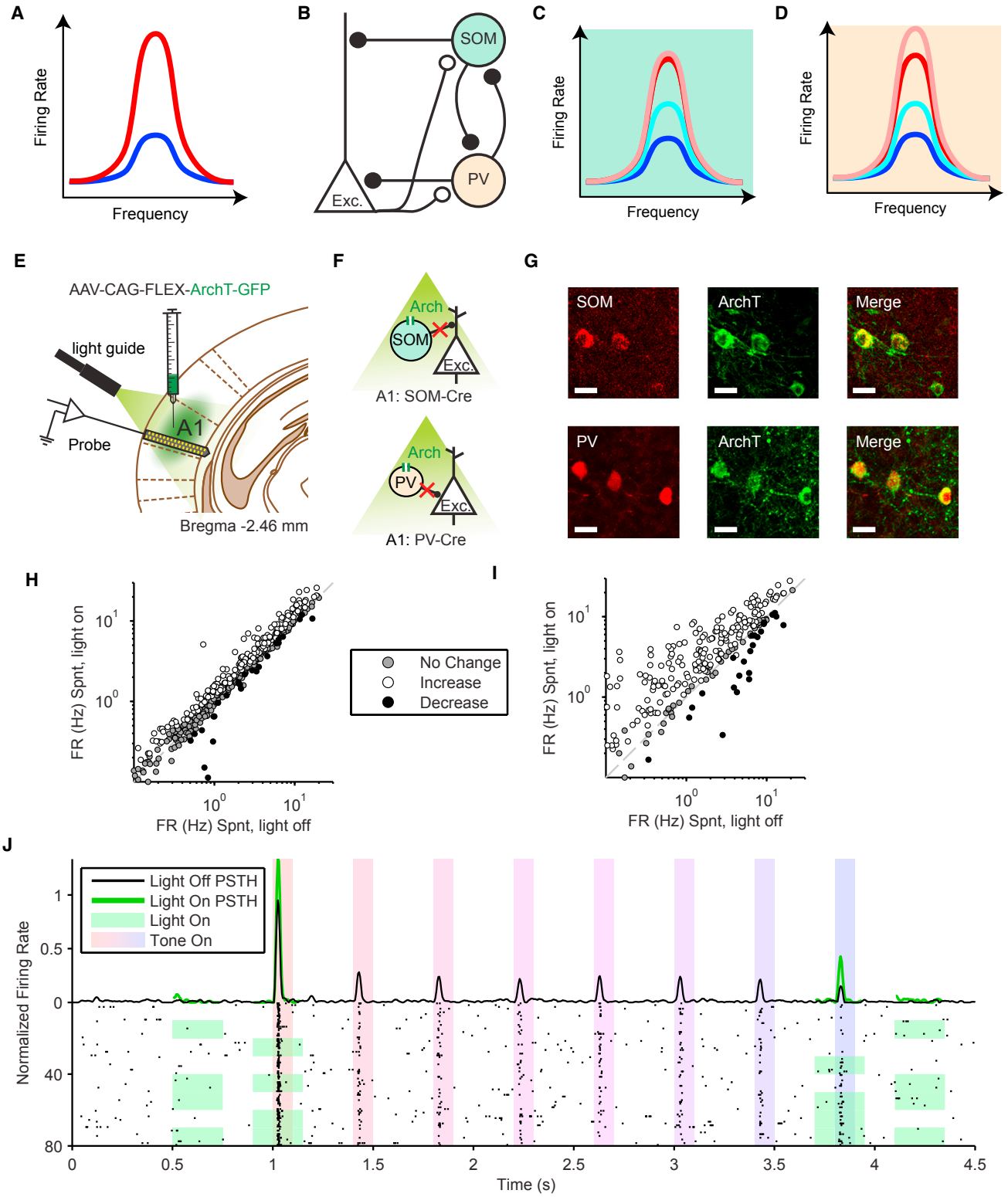

Figure 2. Experimental Design for Testing the Function of Interneurons in Adaptation to Repeated Tones

(A) Diagram of a cortical neuronal frequency response function before (red) and after (blue) adaptation.

(B) Diagram of cortical circuits tested here, illustrating that SOMs and PVs form inhibitory synapses (filled) on the distal dendrites versus soma, respectively, of excitatory neurons (Exc.), which form reciprocal excitatory synapses (open). Additionally, SOMs and PVs inhibit each other.

(legend continued on next page)

Effects of SOM, but Not PV, Inhibition Become Stronger with Adaptation in a Frequency-Selective Fashion

We next tested whether the effects of SOMs or PVs differed for tones in the center (preferred frequencies) and on the sidebands (non-preferred) of the tuning curve of excitatory neurons (Figures 3G–3J). For the first tone (Figures 3G and 3I), suppressing SOMs slightly disinhibited responses only for non-preferred frequencies (non-preferred $p = 2e{-}4$, $t(54) = 4.01$; preferred $p = 0.548$, $t(54) = 0.62$). Yet in the adapted regime, suppressing SOMs preferentially disinhibited responses to tones at preferred frequencies (non-preferred $p = 3e{-}6$, $t(54) = 5.26$; preferred $p = 0.045$, $t(54) = 2.05$; Figures 3H and 3J). Indeed, there was a significant positive shift in the firing rate for preferred frequencies in the suppression-versus-tone frequency curve (slope; $p = 0.031$; $t(54) = 1.91$) and no change in the intercept ($p = 0.155$; $t(54) = 1.02$). These results suggest that SOMs increasingly contribute to adaptation of responses across frequency tuning in a selective fashion (Figures 3K, 3L, 3O, and 3P).

In contrast, suppressing PVs had a stronger disinhibitory effect on neuronal responses at non-preferred tone frequencies than at preferred frequencies during both the first (non-preferred $p = 0.014$, $t(22) = 2.68$; preferred $p = 0.392$, $t(22) = -0.87$) and last tone pips (non-preferred $p = 0.004$, $t(22) = 3.26$; preferred $p = 0.880$, $t(22) = 0.015$; Figures 3I and 3J). Over the population, neither the slope ($p = 0.103$; $t(22) = 1.31$) or intercept ($p = 0.894$; $t(22) = 1.29$) significantly changed from the first to last tone (Figures 3M and 3N). This suggests that PVs preferentially inhibit neuronal responses in the side bands of frequency curves, and their effect is insensitive to adaptation to tone repetition (Figures 3M, 3N, 3Q, and 3R).

Effects of SOM and PV Suppression Differ for Adaptive and Non-adaptive Neurons

To examine how the effects of optogenetic manipulation of SOM or PV activity changed with adaptation for individual neurons, we compared the change in tone-evoked responses of excitatory neurons for the first and last tone among adapting and non-adapting neurons separately (Figures 4 and S2). For the adapting population, neuron-frequency pairs for which the first tone pip evoked significantly stronger spiking than the last pip were included (Figures 4A, 4C, S2A, and S2C). For the non-adapting response population, neuron-frequency pairs were included from neurons in which the first and last tone pip-evoked spiking was not significantly different at any frequency (Figures 4B, 4D, S2B, and S2D). We only detected a small number of neurons that exhibited firing rate (FR) facilitation, rather than adaptation, in response to tone repetition and excluded them from further analysis (2 neurons among PV-Cre and 5 among SOM-Cre populations).

SOM suppression affected first and last tone pip-evoked responses differentially between adaptive and non-adaptive neurons. Among adapting neurons, SOM suppression led to heterogeneous first tone pip-evoked modulation: 30% increased and 34% decreased (Figures 4E and S2E). By contrast, more last tone pip-evoked responses increased (54%) and only a small fraction decreased (2%; Figure S2I). Interestingly, on average, SOM suppression led to significant inhibition of first tone pip-evoked responses ($p = 0.027$; $t(96) = -2.25$) and significant disinhibition of last tone pip-evoked responses ($p = 2e{-}12$; $t(96) = 8.04$; Figures 4I, S2M, and S2Q), showing that the strength of SOM inhibition increased from the first to the last tone pip ($p = 2e{-}11$; $t(96) = 7.63$), as already observed for the subpopulation of adapting tuned neurons (Figures 3G and 3H). Similar to adapting units, non-adapting units were heterogeneously modulated by SOM suppression during the first tone pip (31% increased; 28% decreased; Figures 4F, S2B, S2F, and S2N). Unlike adapting units, non-adapting units continued to respond heterogeneously during the last tone pip (38% increased; 17% decreased; Figures 4F, S2J, and S2R). On average, SOM suppression of non-adapting units evoked no significant change of first ($p = 0.373$; $t(41) = -0.90$) or last tone pip-evoked responses ($p = 0.065$; $t(41) = 1.90$), but the strength of SOM inhibition increased from the first to the last tone pip ($p = 0.027$; $t(41) = 2.29$; Figure 4J).

Similar to SOMs, PV inhibition affected first and last tone pip-evoked responses differentially between adaptive and non-adaptive responses. However, the net effects of PV suppression were weaker than those of SOM suppression. Among adapting units, PV suppression led to heterogeneous first tone pip-evoked modulation (27% increased and 28% decreased; Figures 4C, 4G, 4K, and S2G). For the last tone pip, many responses increased (66%) and a smaller portion decreased (8%; Figure S2K). On average, PV suppression led to significant disinhibition of both first ($p = 0.045$; $t(88) = 2.03$) and last tone pip-evoked responses ($p = 1e{-}13$; $t(88) = 8.75$; Figures S2O and S2S), and the strength of PV inhibition increased from the first to the last tone pip ($p = 1e{-}7$, $t(88) = 5.72$; Figures 4G and 4K). Non-adapting units were heterogeneously modulated by PV suppression during the first tone pip (31% increased; 29% decreased; Figures 4D, 4H, 4L, and S2H) and inhibited more responses during the last tone pip (24% increased; 43% decreased; Figure S2L). On average, PV suppression led to

(C and D) Diagrams of predicted modulatory effects of SOMs (C) and PVs (D) on excitatory neuron tuning curves; before adaptation, suppressing SOMs does not change responses across the tuning curve (pink) but increases responses after adaptation (light blue). Before and after adaptation, suppressing PVs increases responses across the tuning curve.

(E) Diagram of experimental manipulations; AAV-CAG-FLEX-ArchT-GFP was injected in A1. During experiments, neuronal activity was recorded using a multi-channel silicon probe in A1 with an optic fiber for illuminating cortex expressing ArchT.

(F) Green light (532 nm) suppresses SOMs in SOM-Cre mice (top) or PVs in PV-Cre mice (bottom).

(G) Co-expression of ArchT and an interneuron-type reporter in A1. (Top) SOM-Cre mouse A1 is shown. (Bottom) PV-Cre mouse A1 is shown. Green, Arch-GFP; red, anti-body stain for parvalbumin or somatostatin. The scale bar represents 25 μm.

(H and I) Spontaneous firing rate with versus without optogenetic suppression of SOMs (H) or PVs (I). Each dot represents a single neuron and indicates that optogenetic suppression significantly increased (white), decreased (black), or had no effect (gray) on spontaneous firing.

(J) Raster and PSTH of a single neuron's spiking responses with (green) and without optogenetic modulation (black). Green shading in raster plot indicates light pulse times and trials.

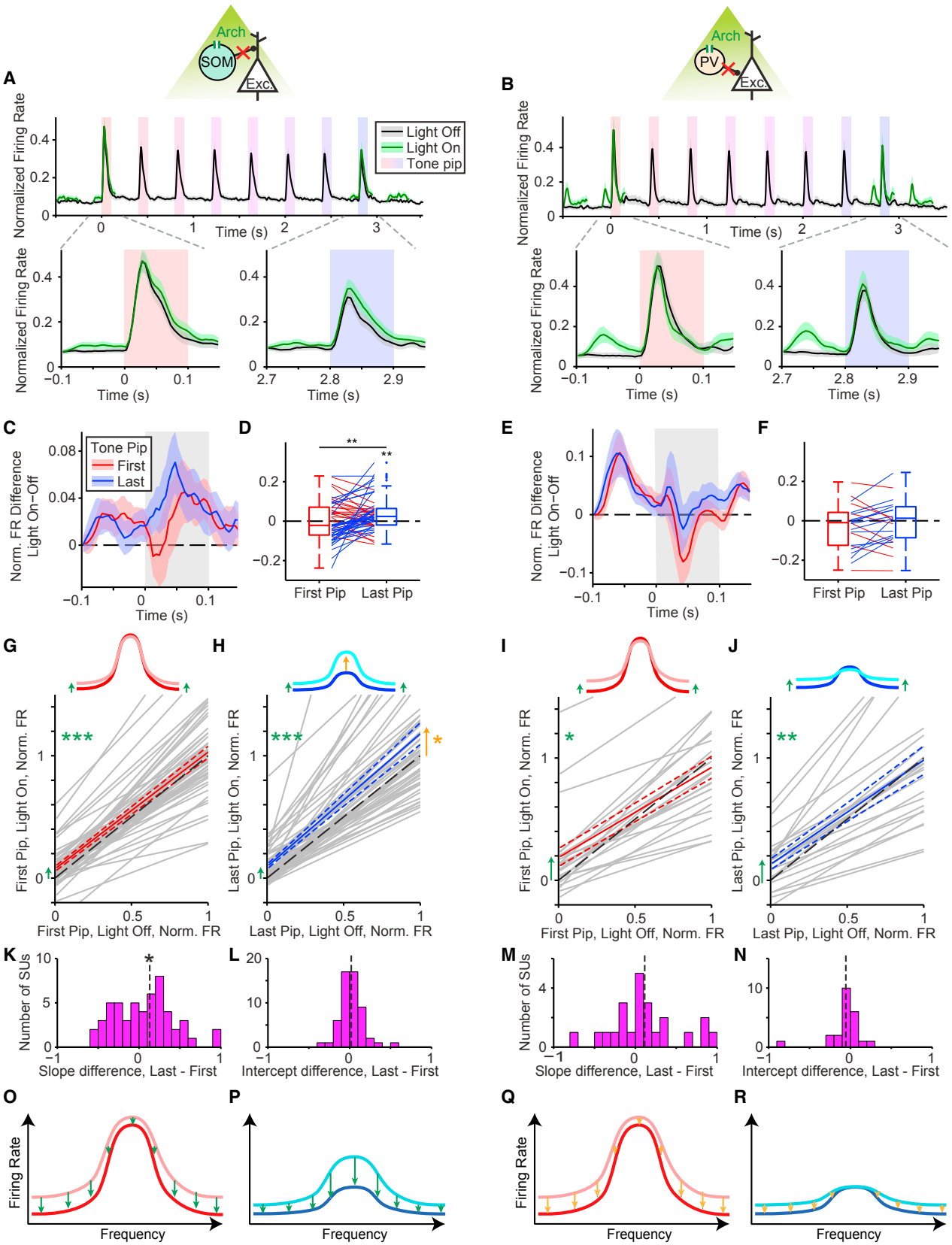

(legend on next page)

just significant disinhibition of first tone pip-evoked responses ($p = 0.043$; $t(40) = 2.09$) and no significant modulation of last tone pip-evoked responses ($p = 0.051$; $t(40) = 2.01$; Figures 4L, S2P, and S2T). The strength of PV inhibition did not change significantly from the first to last tone pip ($p = 0.778$; $t(40) = 0.28$; Figure 4L) for non-adapting units. Thus, PV suppression provided a differential but weaker contribution to adaptation than SOM suppression.

Adaptation Strength of Excitatory Neurons Correlates Differentially with the PV and SOM Modulatory Effects

Does the effect of SOM or PV suppression predict the strength of adaptation? Indeed, the magnitude of adaptation showed a nearly significant correlation with the modulation of the firing rate due to SOM suppression for the first tone ($r = 0.31 \pm 0.18$; $p = 0.044$; $t(173) = 1.71$; $n = 330$), and this correlation grew even stronger and more significant for the last tone ($r = 0.58 \pm 0.08$; $p = 2e{-}11$; $t(173) = 7.03$; $n = 330$; Figures 4M and 4O). The strength of SOM inhibition of each neuron is thus predictive of magnitude of adaptation. By contrast, the magnitude of adaptation was anti-correlated with the modulation of the firing rate due to PV suppression for the first tone ($r = -0.46 \pm 0.19$; $p = 0.008$; $t(149) = -2.46$; $n = 466$) and not correlated for the last tone ($r = 0.14 \pm 0.15$; $p = 0.181$; $t(149) = 0.15$; $n = 466$; Figures 4N and 4P). The strength of FR changes from PV modulation is thus predictive of the magnitude of adaptation, yet suppressing PVs typically drives the firing rate in the opposite direction from SOM. Furthermore, adaptation abolishes this correlation. Together, these results show that inhibition from SOMs, rather than PVs, matches the range of adaptation profiles across the population.

Supporting these observations, the difference in the change in neuronal firing rate due to SOM suppression during the first and last tone was not correlated for adapting neurons ($r = 0.02 \pm 0.08$; $p = 0.0401$; $t(96) = 0.25$; $n = 161$) or non-adapting neurons ($r = 0.19 \pm 0.13$; $p = 0.075$; $t(40) = 1.47$; $n = 66$; Figures S3A and S3C). These correlations demonstrate that the sign and magnitude of SOM inhibition can change over repeated stimulation, especially for neurons that significantly adapt. By contrast, the effect of PV suppression between the first and last tone was strongly correlated for both adapting units ($r = 0.26 \pm 0.06$; $p = 1e{-}5$; $t(88) = 4.42$; $n = 186$) and non-adapting units ($r = 0.37 \pm 0.08$; $p = 4e{-}5$; $t(39) = 4.45$; $n = 101$; Figures S3B and S3D). This result shows that the sign and magnitude of PV inhibition is largely insensitive to stimulus repetition or magnitude of adaptation. Together, these results show that neurons that experience stronger SOM inputs are more likely to adapt strongly, whereas modulation of activity by PVs is not affected by adaptation.

Both SOMs and PVs Affect Excitatory Neuronal Activity More Strongly after Adaptation

We hypothesized that the observed effects could be explained by changes in connectivity strength between the inhibitory and excitatory neurons before and after adaptation. To approximate how strongly excitation of inhibitory neurons affect responses in excitatory neurons, we drove either SOMs or PVs to express an ultrafast channelrhodopsin (ChETA) and used brief light pulses to elicit spiking in these interneurons (Figures 5A–5D and S4A). Brief pulses of light elicited reliable spikes within 3–7 ms of laser onset in a subset of neurons, indicating that light activated those neurons directly (Figures 5B, 5C, and S4B–S4E).

We recorded responses of excitatory and inhibitory neurons in awake mice presented with sequences of repeated trains, each composed of one of two chosen tone frequencies, while projecting light on auditory cortex (AC) either before the tone train, during the first tone, during the last tone, or after the tone train (Figure 5D). The timing of light activation was designed to elicit the volley of inhibitory activity just preceding the cortical response to the tone in excitatory neurons: the light pulse lasted from 5 to 7.5 ms after tone onset. This produced an elevated spiking activity in putative inhibitory neurons around 7–12 ms after tone onset, just before the typical tone-evoked activity, and suppressed tone-evoked activity (Figures S4B and S4C). In some putative excitatory neurons, activating PVs or SOMs resulted in nearly full suppression of tone-evoked activity (Figures 5E and 5F). The FR elicited by the light pulse was not significantly different between the first and last tones for SOM-Cre mice (0.5 ± 0.3 Hz; $p = 0.066$; $t(304) = 1.84$) or PV-Cre mice (0.0 ± 0.4; $t(369) = 0.10$; Figures S4D and S4E).

Figure 3. SOM Inhibition Increases with Stimulus Repetition and Contributes to Scaling after Adaptation whereas PV Inhibition Is Stable across Adaptive Regimes

For a Figure360 author presentation of Figure 3, see the figure legend at https://doi.org/10.1016/j.celrep.2017.10.012.

(A and B) Selected neuron (F and G) population mean firing rate in response to tone trains with (green) and without (black) optogenetic suppression of SOMs (A) and PVs (B). (Top) PSTH over whole tone train is shown. (Bottom) First (left) and last (right) pips are shown.

(C and E) PSTHs of the mean per-neuron difference in firing rate between trials with and without optogenetic suppression of SOMs (C) and PVs (E) for the first (red) and last (blue) pip. Grey shaded region indicates tone on time. For light-on trials, illumination lasted the entire duration of the PSTH window.

(D and F) Per-neuron mean differences in firing rate between trials with and without optogenetic suppression in the first and last tone onset response for SOMs (D) and PVs (F). Line color indicates increased (blue) or decreased (red) firing rate from the first to last pip.

(G–J) (Top) Diagram of tuning curve in response to the first (red) and last (blue) tone pip with (light) and without (dark) optogenetic suppression of SOMs (G and H) or PVs (I and J). (Bottom) Linear fits to the first (G and I) or last (H and J) tone pip firing rate responses in selected neurons, with versus without optogenetic suppression for each neuron (gray) and population mean (color). Arrows emphasize significant changes in non-preferred (green) or preferred (orange) frequencies.

(K–N) Slope (K and M) and intercept (L and N) of linear fits for selected neurons and population mean (line) in SOM-Cre mice (K and L) or PV-Cre mice (M and N), respectively.

(O–R) Model of typical pyramidal neuron frequency response function in a non-adapted (O and Q) and adapted (P and R) regime (dark) as a combination of excitatory response (light) and inhibitory suppression from SOM (green) or PV interneurons (orange).

See also Figure S1.

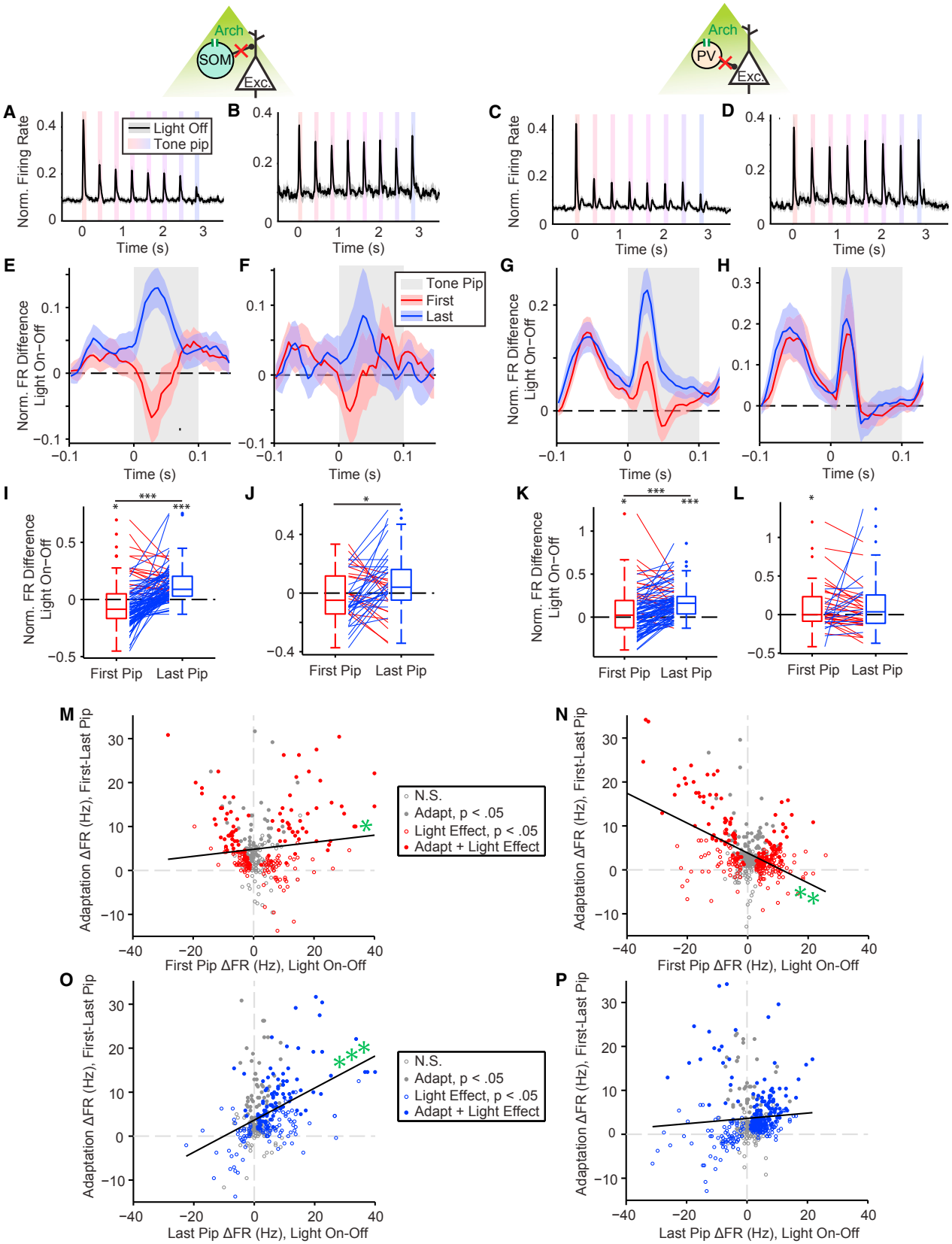

(legend on next page)

If the synapses between inhibitory and excitatory neurons were facilitated after adaptation, eliciting the same number of spikes in inhibitory neurons should drive stronger changes in excitatory neuronal activity after adaptation. Indeed, we found that briefly activating SOMs or PVs elicited relatively greater change in excitatory neuron activity during tone-evoked responses (SOM, 0.07 ± 0.03, p = 0.0496, t(226) = 1.97; PV, 0.15 ± 0.03, p = 1.5e−6, t(275) = 4.9; Figures 5G and 5I). These findings suggest that the relative suppression from either inhibitory neuron becomes stronger after adaptation.

However, there were several caveats to this experiment. When we computed the firing rate difference rather than the relative index of change, we found that SOM and PV activation inhibited more spiking during the first tone compared to the last tone (SOM, −1.3 ± 0.2 Hz, p = 2.7e−7, t(270) = −5.2; PV, −0.6 ± 0.2 Hz, p = 5.2e−4, t(320) = −3.5; Figures 5H and 5J). This result can be explained by the floor effect of near complete suppression of excitatory neuronal response. Additionally, there was no significant difference in the relative effects of PV or SOM activation on the spontaneous firing rate—likely due to the low spontaneous firing rate of the neurons (SOM, 0.01 ± 0.03, p = 0.743, t(170) = 0.32; PV, −0.00 ± 0.04, p = 0.93, t(255) = −0.06; Figures S4F and S4H). As measured by the difference in firing rate, SOM and PV activation inhibited more spontaneous spikes before compared to after the tone train but this likely due to reduced spontaneous activity following adaptation, similar to the effects during tone-evoked activity described above (SOM, −0.9 ± 0.1 Hz, p = 9e−18, t(269) = −9.2; PV, −0.5 ± 0.1, p = 2e−8, t(280) = −5.78; Figures S3G and S3I), likely due to floor effects. Combined, the results suggest that inhibition due to single spike produced by either PVs and SOMs becomes relatively, but not absolutely, stronger with adaptation.

DISCUSSION

Our study dissected the complex roles of cortical inhibitory interneurons in adaptation to repeated sounds, identifying the differences in the contributions of two distinct interneuron subtypes, SOMs and PVs (Rudy et al., 2011). Cortical inhibitory interneurons are thought to play a crucial role in information processing and to shape how information is represented and transmitted within and between cortical neuronal populations (Yuste, 2015). Molecularly distinct classes of interneurons are proposed to exert differential functions in information processing (Kepecs and Fishell, 2014; Markram et al., 2004; Rudy et al., 2011). Yet despite the differential morphology of the neurons, determining the differences in the action of PVs and SOMs in auditory cortical processing has proven elusive using static stimuli. Suppressing or activating PVs and SOMs during tone presentation led to a range of multiplicative and linear offset effects on excitatory tone-evoked responses (Aizenberg et al., 2015; Phillips and Hasenstaub, 2016; Seybold et al., 2015).

Interestingly, PV and SOM modulation produces consistent differences when the temporal dimension of responses is explored. SOMs respond to tones with a greater delay than PVs (Li et al., 2015; Moore and Wehr, 2013). Furthermore, SOMs, but not PVs, exert enhanced inhibition in accordance with behavioral habituation to stimuli over a timescale of days (Kato et al., 2015). In our study, we find that SOM-mediated inhibition, but not PV-mediated inhibition, is specific to temporal adaptation over a timescale of seconds. The effect of PV modulation is highly correlated from first to last tone pip, for both adaptive and non-adaptive neuronal responses (Figures S3B and S3D). This means that PVs tend to exert the same type of modulatory effect across the time course of the tone train, suggesting that PVs are not affected by stimulus-history conditions. By contrast, SOM-mediated modulation effects on adaptive responses are more weakly correlated from first to last tone pip and not correlated in non-adaptive responses (Figures S3A and S3C). SOMs generally become more inhibitory after the tone train, suggesting that SOMs are strongly affected by stimulus-history conditions (Figures 3 and 4). Additionally, the strength of SOM inhibitory influence on excitatory responses correlates with the magnitude of adaptation (Figures 4M–4P), i.e., SOMs more strongly inhibit neurons that adapt strongly. By contrast, PVs inhibit non-adapting neurons more strongly, at least during the first tone pip (Figures 3 and 4). Our present results demonstrate that SOMs dynamically control tone-evoked responses both across the spectral and temporal dimensions, whereas PVs provide a temporally uniform drive. The differential temporal and context-dependent effects may underlie the more fundamental distinction between the function of PVs and SOMs in sensory processing, which relies on long-term temporal integration.

What are the network mechanisms driving these differential changes in SOM inhibition during adaptation? A top candidate would be facilitation at the SOM to excitatory neuron synapse (Reyes et al., 1998; Silberberg and Markram, 2007). Consistently, we found that eliciting a brief burst of spikes in either PVs or SOMs predictably elicited suppression in excitatory

Figure 4. Effects of Optogenetic Modulation of SOMs and PVs on Adaptive versus Non-adaptive Neurons

(A–D) Population mean firing rate PSTH in response to tone trains for adaptive (A and C) and non-adaptive neuronal responses (B and D) among the SOM-Cre (A and B) or PV-Cre populations (C and D).

(E–H) PSTHs of mean per-neuron difference in firing rate between trials with and without optogenetic suppression of interneurons for the first (red) and last (blue) pip for adaptive (E and G) and non-adaptive neuronal responses (F and H) among the SOM-Cre (E and F) or PV-Cre populations (G and H).

(I–L) Summary of the per-neuron difference in firing rate between trials with and without optogenetic suppression of interneurons in the first and last tone onset response for adaptive (I and K) and non-adaptive neuronal responses (J and L) among the SOM-Cre (I and J) or PV-Cre populations (K and L).

(M–P) Effect of SOM (M and O) or PV (N and P) optogenetic suppression on firing rates for all neurons in response to the first (M and N) or last (O and P) tone pip versus the magnitude of firing rate adaptation. Optogenetic effects are measured as difference between the means of trials with and without optogenetic suppression. Adaptation is measured as the difference between firing rate in response to the first and last pip. Each dot represents a neuron frequency pair. Dot color and fill indicate significant optogenetic modulation or adaptation, respectively. Asterisks, significance of correlation coefficient of cluster-robust regression; black, ordinary least-squares fit.

See also Figures S2 and S3.

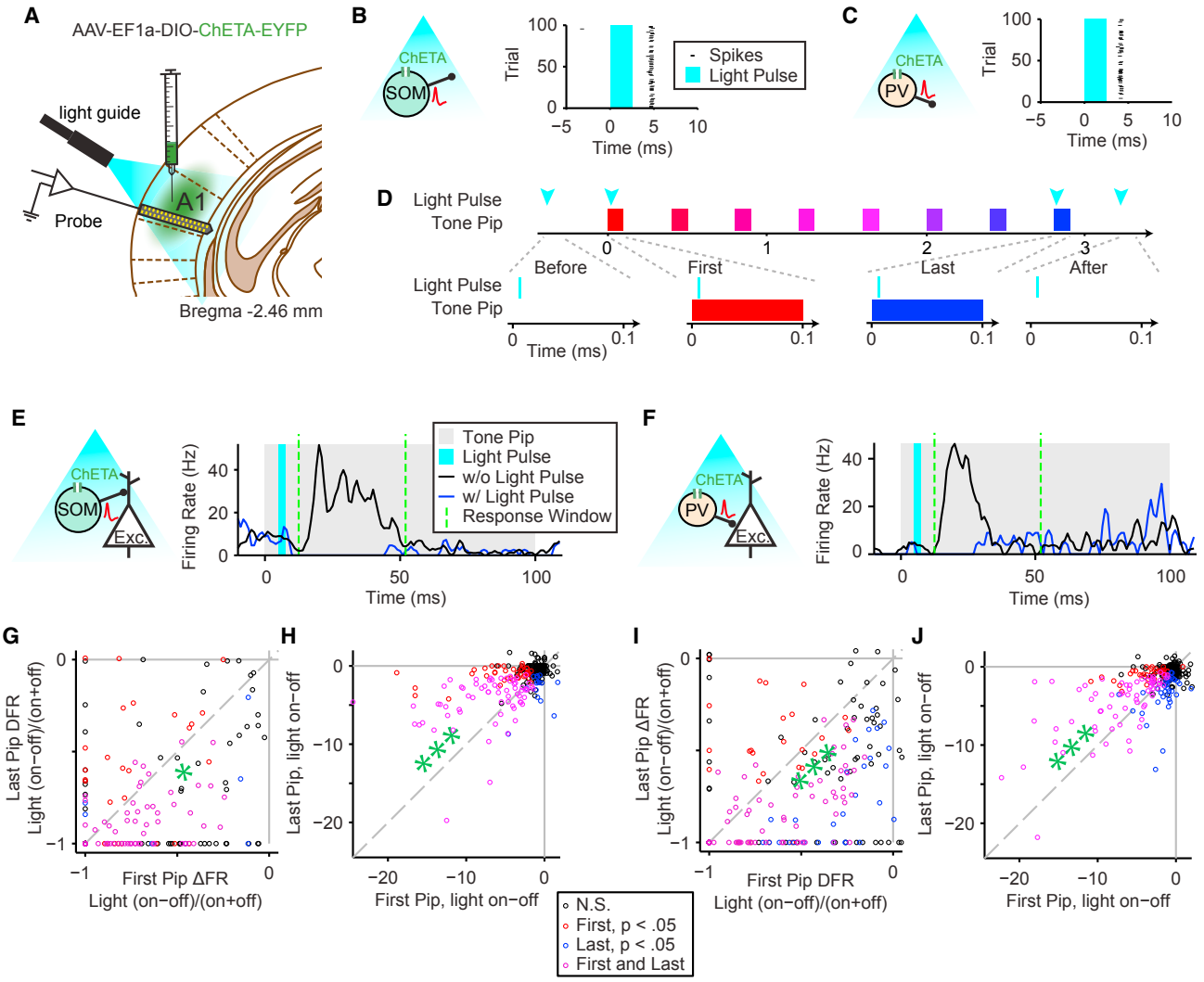

Figure 5. Effects of Brief SOM or PV Activation on Tone-Evoked Responses before and after Adaptation

(A) Diagram of experimental manipulations; AAV-EF1a-DIO-ChETA-EYFP was injected in A1. During experiments, neuronal activity was recorded using a multi-channel silicon probe in A1 with an optic fiber for illuminating cortex expressing ArchT.

(B and C) (Left) Blue light (430 nm) activates SOMs (B) or PVs (C). (Right) Raster shows a single-neuron spiking response to 2.5-ms light pulses.

(D) Diagram of tone trains and light pulses. (Top) 2.5-ms light pulses may occur at one of four time points during each trial; before or after the train or during the first or last tone pip. (Bottom) Zoom in of pulse timings is shown.

(E and F) PSTHs of a single-neuron mean tone-evoked response with and without optogenetic activation of SOMs (E) or PVs (F). Green, analysis window 13–52 ms.

(G–J) Index of change (G and I) or difference (H and J) between responses with and without optogenetic activation for first versus last tone-evoked firing rate. One circle per neuron, color indicates significance of modulation between conditions. Asterisks above or below unity line indicate a significant increase or decrease in population firing rates.

See also Figure S4.

neurons, which was relatively stronger after adaptation (Figures 5 and S4). However, multiple alternative mechanisms may underlie the observed phenomenon. First, repeated activation of facilitating synapses between SOMs and local pyramidal neurons may lead to increased inhibition relative to excitation, despite reduced spiking. Second, a distinct subpopulation of SOMs for which stimulus-evoked responses increase with repetition may entirely generate the observed increase in inhibition. Third, stimulus-specific reduced firing rates among SOMs may disinhibit PVs relative to pyramidal neurons, leading to increased inhibition. Fourth, SOMs may relay a top-down or modulatory signal generated elsewhere that drives greater inhibition in specific stimulus contexts (Kuchibhotla et al., 2017; Pi et al., 2013). Testing each of these possibilities is required to disambiguate the specifics of the synaptic changes over the timescale of adaptation.

Combined, our results define functional characteristics that differentiate SOMs versus PVs: SOMs appear to play a

generalized role and likely underlie cortical adaptation to repeated stimuli, especially for well-tuned stimuli, whereas PVs do not. Because adaptation is observed in every primary sensory cortex and is likely a canonical computation of all cortical regions, our results point to the unique and generalized adaptive role SOM inhibition may play in canonical cortical circuitry.

EXPERIMENTAL PROCEDURES

Animals

All experiments were performed in adult male mice (supplier, Jackson Laboratories; age, 12–15 weeks; weight, 22–32 g; PV-Cre mice, strain: B6;129P2-Pvalbtm1(cre)Arbr/J; SOM-Cre: Ssttm2.1(cre)Zjh/J) housed at 28°C on a 12 hr light:dark cycle with water and food provided ad libitum. In PV-Cre mice, Cre recombinase (Cre) is expressed in parvalbumin-positive interneurons; in SOM-Cre mice, Cre is expressed in somatostatin-positive interneurons (Taniguchi et al., 2011). This study was performed in strict accordance with the recommendations in the Guide for the Care and Use of Laboratory Animals of the NIH. All of the animals were handled according to a protocol approved by the Institutional Animal Care and Use Committee of the University of Pennsylvania (protocol number: 803266). All surgery was performed under isoflurane anesthesia, and every effort was made to minimize suffering.

Viral Vectors

Modified AAVs encoding ArchT (AAV-CAG-FLEX-ArchT-GFP; UNC Vector Core) or ChETA (AAV-EF1a-DIO-ChETA-EYFP) were used for selective suppression or excitation, respectively, in PV-Cre or SOM-Cre mice.

Virus Injection

2–4 weeks prior to the start of experimental recordings, a 0.5-mm-diameter craniotomy was drilled over primary auditory cortex (2.6 mm caudal and 4.1 mm lateral from bregma) under aseptic conditions while the mouse was anesthetized with isoflurane. A 750-nL bolus of AAV in water was injected into A1 (1 mm ventral from pia mater) using a stereotaxic syringe pump (Pump 11 Elite Nanomite; Harvard Apparatus). The skull overlying A1 was thinned by gentle drilling. The craniotomy was covered with bone wax, and a small custom head post was secured to the skull with dental acrylic.

Electrophysiological Recordings

All recordings were carried out inside a double-walled acoustic isolation booth (Industrial Acoustics). Electrodes were targeted to A1 on the basis of stereotaxic coordinates and relation to blood vessels. In electrophysiological recordings, the location was confirmed by examining the click and tone pip responses of the recorded units for characteristic responses of neurons in A1, as described previously by our group in the rat (Blackwell et al., 2016; Carruthers et al., 2013, 2015; Natan et al., 2017) and in the mouse (Aizenberg et al., 2015; Natan et al., 2015). Mice were placed in the recording chamber, anesthetized with isoflurane, and the head post secured to a custom base, immobilizing the head. Dental acrylic and bone wax was gently drilled away, exposing auditory cortex, and a silicon multi-channel probe (A1x32-tri-5mm-91-121-A32; Neuronexus) was slowly lowered to between 900 μL and 1,100 mm into cortex, perpendicularly to the cortical surface. Electrophysiological data from 32 channels were bandpass filtered at 10–300 Hz for local field potential (LFP) and current-source density (CSD) analysis or at 600–6,000 Hz for spike analysis, digitized at 32 kHz and stored for offline analysis (Neuralynx). Spikes belonging to single units were clustered using commercial software (Offline Sorter; Plexon; Carruthers et al., 2013). Putative excitatory neurons were identified based on their expected response patterns to sounds and lack of significant suppression of the spontaneous firing rate due to light (Lima et al., 2009; Moore and Wehr, 2013).

Acoustic Stimulus

Stimuli were delivered via a magnetic speaker (Tucker-David Technologies) directed toward the mouse's head. Speakers were calibrated prior to the experiments to ±3 dB over frequencies between 1 and 40 kHz by placing a microphone (Brüel and Kjaer) in the location of the ear contralateral to the recorded A1 hemisphere, recording speaker output and filtering stimuli to compensate for acoustic aberrations (Carruthers et al., 2013). First, to measure tuning, a train of 50 pure tones of frequencies spaced logarithmically between 1 and 80 kHz, at 65 dB sound pressure level relative to 10 microPascals (SPL) relative to 20 μPa, in pseudo-random order was presented 20 times. Each tone was 100 ms long (5-ms cosine squared ramped up and down) with an inter-stimulus interval (ISI) of 300 ms. Frequency response functions were calculated online for several multiunits. To construct the set of tone pip trains, 10 frequencies, spaced 0.13 octave apart, were selected to cover a portion of multiunit frequency tuning curve from preferred to non-preferred frequencies. Because many neurons were tested simultaneously, the chosen test frequencies effectively sampled different portions of the tuning curve for different neurons in each experimental session. The tone frequencies were selected to overlap with the most neuronal frequency response areas but did not exactly fall within the same frequency region of each neuron's tuning curve. Each tone train consisted of 8 consecutive 100-ms tone pips of the same frequency separated by 300 ms ISI. The frequency of each train was pseudorandom and counterbalanced. Trains were separated by 2.4 s of silence to allow adaptation to reverse (Figure 1B). Whereas cortical neurons adapt across a range of tone repeat rates (Ulanovsky et al., 2004), a relatively long (300 ms) inter-tone interval was chosen to incorporate the time course of optogenetic stimulation, enable comparison of results to prior studies (Natan et al., 2015), and target long-term adaptation, likely affected by intra-cortical feedback mechanisms, which take place over hundreds of milliseconds (Kato et al., 2015; Natan et al., 2015).

Light Presentation

An optic fiber was use to direct 532-nm or 473-nm laser light (Shanghai Laser and Optics Century). After positioning the silicon probe, an optic fiber was placed over the surface of auditory cortex. To limit Becquerel effect artifacts due to light striking electrodes, we positioned the optical fiber parallel to the silicon probe (Han et al., 2009). For each train, light may be cast over AC with 50% probability during each of 4 time periods: during the first tone; the last tone; or during the silent period 400 ms before or 400 ms after the train. For ArchT-mediated suppression, 532 nm light onset was 100 ms prior to tone onset and lasted for 250 ms. For ChETA-mediated excitation, 473 nm light onset was 5 ms after tone onset and lasted for 2.5 ms. At 180 mW/mm^2, light pulses were intense enough to significantly modulate multiunit activity throughout all cortical layers.

Immunohistochemistry

Viral expression was confirmed post mortem via immunohistochemistry (Figures 2G and S4A), consistent with previous results in our laboratory (Aizenberg et al., 2015; Natan et al., 2015). Brains were post-fixed in paraformaldehyde (PFA) (4%) and cryoprotected in 30% sucrose. Coronal sections (50 μm) for PV were cut using a cryostat (Leica CM1860), and SOMs were cut using a vibratome (Vibratome 1000). Sections were washed in PBS containing 0.1% Triton X-100 (PBST) (3 washes; 5 min), incubated at room temperature in blocking solution (for PV 10% normal goat serum and 5% BSA in PBST for 3 hr; for SOM 1% normal horse serum with 0.1% BSA and 0.5% Triton X-100 in PBS for 1 hr), and then incubated in primary antibody diluted in blocking solution overnight at 4°C. The following primary antibodies were used: anti-PV (PV 25 rabbit polyclonal; 1:500; Swant) or anti-SOM (MAB354 rat monoclonal; 1:200; Millipore; clone YC7). After incubation, sections were washed in blocking solution (3 washes; 5 min), incubated for 2 hr at room temperature with secondary antibodies (Alexa Fluor 594 goat anti-rabbit immunoglobulin G [IgG] 1:1,000 for PV and Alexa Fluor 568 goat anti-rat IgG 1:750 for SOM), and then washed in PBS (3 washes; 5 min each). Sections were mounted using Fluoromount-G (Southern Biotech), and confocal images were acquired (Leica SP5).

In Vivo Neuronal Response Analysis

Neuron Frequency Pairs

Termed neuron frequency pairs, each of the 10 frequencies used in the tone pip trains was tested separately for various trial-by-trial FR features for inclusion and exclusion from specific population analyses: tone-evoked FR greater than 1 Hz; significantly greater tone-evoked responses compared to spontaneous activity; significant changes in FR in response to optogenetic illumination; and significant differences between first and last tone-evoked FR.

FR Analyses

Population post-stimulus time histograms (PSTHs) were calculated by first finding each neuron's mean FR over pooled spike counts across all included frequencies, normalizing by the mean peak FR in response to the first tone pip light-off condition, and then finding the mean across the neurons included in that population. Error bars represent SE. Tone-evoked FRs displayed in box and whisker plots were measured as the mean FR of each neuron between 10 ms and 40 ms after tone onset. In scatterplots, each dot represents a neuron frequency pair mean FR between 10 ms and 40 ms after tone onset. Spontaneous activity before tone pip trains was measured from 400 ms to 350 ms before the first tone onset, and spontaneous activity after tone pip trains was measured from 400 ms to 450 ms after the last tone onset. We compared the effects of SOM or PV suppression on excitatory responses to tones across the entire tuning curve for either the first (Figures 3G and 3I) or last tone (Figures 3H and 3J). If inhibitory neurons contribute to adaptation, we expect the magnitude of adaptation to correlate with the strength of response modulation due to interneuron suppression. In order to test this, we measured the correlation between the magnitude of adaptation, indexed by firing rate before and after inhibition, with the inhibition strength, indexed by firing rate with and without interneuron suppression, for several frequencies across neurons. To compensate for correlations between multiple samples from each neuron, we used cluster-robust SE to measure regression (Cameron and Miller, 2015).

Linear Fits across Frequencies

Linear fits were calculated using linear regression (fitlm.m; MATLAB) over 10 data points, one for each of the 10 frequencies tested. For each comparison condition (first or last tone pip response, with or without optogenetic suppression), the 10 data points were separately calculated as the mean FR over all repeats fitting those conditions. Linear fit error lines indicate SE. Population average line was calculated as the mean of each line's y value across x from 0 to 1, and error bars show SE.

Limitations of the Study Design

Some aspects of this study limit the extent to which the results may generalize. One limitation is that we only explored adaptation for a single temporal regime, with tones repeated at the rate of 2.5 Hz. Increasing the rate of tone presentation would potentially lead to a faster and stronger adaptation (Ulanovsky et al., 2003), which may recruit different intra-cortical circuits. Another limitation is that optogenetic manipulation did not allow for complete shutdown of interneuron activity (Figures 2H and 2I). Therefore, we measured the effect of modulatory changes and reduced dynamic range of evoked spiking from interneurons rather than measuring the consequence of entirely removing a circuit element from the network. Future studies could extend these experiments focusing on the questions of adaptation dynamics by due to changes in inter-tone interval, timing, and strength of optogenetic modulation.

Statistical Methods

Sign rank tests were used to test whether first or last tone pip-evoked FRs or spontaneous FRs per trial were different within single neurons and used for classification and population inclusion criteria. Rank sum tests were used to test FR differences between light conditions per trial within single neurons and used for classification and population inclusion criteria. All population comparisons were tested using the Student's t test. Correlations were measured across neuron frequency pairs treated as separate samples in order to allow the dataset to reflect preferred and non-preferred frequencies. Because neuron frequency pairs from the same neuron likely exhibit correlation, we used cluster-robust regression to compensate for a possible lack of independent sampling. Clustering samples y neuron adjusts the degrees of freedom, t-value, p value, and corrected correlation coefficient r. In all figures and tests, single, double, and triple stars indicate $p < 0.05$, 0.01, and 0.001, respectively. Unless otherwise indicated, n refers to the number of units included in the analysis.

SUPPLEMENTAL INFORMATION

Supplemental Information includes four figures and can be found with this article online at https://doi.org/10.1016/j.celrep.2017.10.012.

AUTHOR CONTRIBUTIONS

R.G.N. and M.N.G. designed the experiments, analyzed the data, and wrote the paper. R.G.N. and W.R. carried out the experiments.

ACKNOWLEDGMENTS

This work was supported by NIH (grant numbers NIH R03DC013660, NIH R01DC014700, and NIH R01DC015527), Klingenstein Award in Neuroscience, Human Frontier in Science Foundation Young Investigator Award (grant number RGY0073/2014), and the Pennsylvania Lions Club Hearing Research Fellowship to M.N.G. M.N.G. is the recipient of the Burroughs Wellcome Award at the Scientific Interface. R.G.N. was supported by NIH (grant number NIH NIMH T32MH017168). We thank members of the Geffen laboratory and the Hearing Research Center at the University of Pennsylvania for helpful discussions, including Dr. Steve Eliades, Yale Cohen, Mark Aizenberg, Christopher Angeloni, Jennifer Blackwell, and Katherine Wood. We thank Dr. Naoru Koizumi (George Mason University) for helpful conversations and advice on statistical methods.

Received: April 23, 2017
Revised: August 7, 2017
Accepted: October 3, 2017
Published: October 24, 2017

REFERENCES

Abbott, L.F., Varela, J.A., Sen, K., and Nelson, S.B. (1997). Synaptic depression and cortical gain control. Science *275*, 220–224.

Aizenberg, M., Mwilambwe-Tshilobo, L., Briguglio, J.J., Natan, R.G., and Geffen, M.N. (2015). Bidirectional regulation of innate and learned behaviors that rely on frequency discrimination by cortical inhibitory neurons. PLoS Biol. *13*, e1002308.

Blackwell, J.M., Taillefumier, T.O., Natan, R.G., Carruthers, I.M., Magnasco, M.O., and Geffen, M.N. (2016). Stable encoding of sounds over a broad range of statistical parameters in the auditory cortex. Eur. J. Neurosci. *43*, 751–764.

Cameron, A.C., and Miller, D.L. (2015). A practitioner's guide to cluster-robust inference. J. Hum. Resour. *50*, 317–372.

Carruthers, I.M., Natan, R.G., and Geffen, M.N. (2013). Encoding of ultrasonic vocalizations in the auditory cortex. J. Neurophysiol. *109*, 1912–1927.

Carruthers, I.M., Laplagne, D.A., Jaegle, A., Briguglio, J.J., Mwilambwe-Tshilobo, L., Natan, R.G., and Geffen, M.N. (2015). Emergence of invariant representation of vocalizations in the auditory cortex. J. Neurophysiol. *114*, 2726–2740.

Chen, I.W., Helmchen, F., and Lütcke, H. (2015). Specific early and late oddball-evoked responses in excitatory and inhibitory neurons of mouse auditory cortex. J. Neurosci. *35*, 12560–12573.

Dahmen, J.C., Keating, P., Nodal, F.R., Schulz, A.L., and King, A.J. (2010). Adaptation to stimulus statistics in the perception and neural representation of auditory space. Neuron *66*, 937–948.

Geffen, M.N., de Vries, S.E., and Meister, M. (2007). Retinal ganglion cells can rapidly change polarity from off to on. PLoS Biol. *5*, e65.

Han, X., Qian, X., Bernstein, J.G., Zhou, H.H., Franzesi, G.T., Stern, P., Bronson, R.T., Graybiel, A.M., Desimone, R., and Boyden, E.S. (2009). Millisecond-timescale optical control of neural dynamics in the nonhuman primate brain. Neuron *62*, 191–198.

Isaacson, J.S., and Scanziani, M. (2011). How inhibition shapes cortical activity. Neuron *72*, 231–243.

Kato, H.K., Gillet, S.N., and Isaacson, J.S. (2015). Flexible sensory representations in auditory cortex driven by behavioral relevance. Neuron *88*, 1027–1039.

Kepecs, A., and Fishell, G. (2014). Interneuron cell types are fit to function. Nature *505*, 318–326.

Kuchibhotla, K.V., Gill, J.V., Lindsay, G.W., Papadoyannis, E.S., Field, R.E., Sten, T.A., Miller, K.D., and Froemke, R.C. (2017). Parallel processing by

cortical inhibition enables context-dependent behavior. Nat. Neurosci. *20*, 62–71.

Li, L.Y., Ji, X.Y., Liang, F., Li, Y.T., Xiao, Z., Tao, H.W., and Zhang, L.I. (2014). A feedforward inhibitory circuit mediates lateral refinement of sensory representation in upper layer 2/3 of mouse primary auditory cortex. J. Neurosci. *34*, 13670–13683.

Li, L.Y., Xiong, X.R., Ibrahim, L.A., Yuan, W., Tao, H.W., and Zhang, L.I. (2015). Differential receptive field properties of parvalbumin and somatostatin inhibitory neurons in mouse auditory cortex. Cereb. Cortex *25*, 1782–1791.

Lima, S.Q., Hromádka, T., Znamenskiy, P., and Zador, A.M. (2009). PINP: a new method of tagging neuronal populations for identification during in vivo electrophysiological recording. PLoS ONE *4*, e6099.

Ma, Y., Hu, H., Berrebi, A.S., Mathers, P.H., and Agmon, A. (2006). Distinct subtypes of somatostatin-containing neocortical interneurons revealed in transgenic mice. J. Neurosci. *26*, 5069–5082.

Markram, H., Toledo-Rodriguez, M., Wang, Y., Gupta, A., Silberberg, G., and Wu, C. (2004). Interneurons of the neocortical inhibitory system. Nat. Rev. Neurosci. *5*, 793–807.

Moore, A.K., and Wehr, M. (2013). Parvalbumin-expressing inhibitory interneurons in auditory cortex are well-tuned for frequency. J. Neurosci. *33*, 13713–13723.

Natan, R.G., Briguglio, J.J., Mwilambwe-Tshilobo, L., Jones, S.I., Aizenberg, M., Goldberg, E.M., and Geffen, M.N. (2015). Complementary control of sensory adaptation by two types of cortical interneurons. eLife *4*, e09868.

Natan, R.G., Carruthers, I.M., Mwilambwe-Tshilobo, L., and Geffen, M.N. (2017). Gain control in the auditory cortex evoked by changing temporal correlation of sounds. Cereb. Cortex *27*, 2385–2402.

Phillips, E.A., and Hasenstaub, A.R. (2016). Asymmetric effects of activating and inactivating cortical interneurons. eLife *5*, e18383.

Pi, H.J., Hangya, B., Kvitsiani, D., Sanders, J.I., Huang, Z.J., and Kepecs, A. (2013). Cortical interneurons that specialize in disinhibitory control. Nature *503*, 521–524.

Reyes, A., Lujan, R., Rozov, A., Burnashev, N., Somogyi, P., and Sakmann, B. (1998). Target-cell-specific facilitation and depression in neocortical circuits. Nat. Neurosci. *1*, 279–285.

Rudy, B., Fishell, G., Lee, S., and Hjerling-Leffler, J. (2011). Three groups of interneurons account for nearly 100% of neocortical GABAergic neurons. Dev. Neurobiol. *71*, 45–61.

Schwartz, O., and Simoncelli, E.P. (2001). Natural signal statistics and sensory gain control. Nat. Neurosci. *4*, 819–825.

Seybold, B.A., Phillips, E.A., Schreiner, C.E., and Hasenstaub, A.R. (2015). Inhibitory actions unified by network integration. Neuron *87*, 1181–1192.

Silberberg, G., and Markram, H. (2007). Disynaptic inhibition between neocortical pyramidal cells mediated by Martinotti cells. Neuron *53*, 735–746.

Solomon, S.G., and Kohn, A. (2014). Moving sensory adaptation beyond suppressive effects in single neurons. Curr. Biol. *24*, R1012–R1022.

Taniguchi, H., He, M., Wu, P., Kim, S., Paik, R., Sugino, K., Kvitsiani, D., Fu, Y., Lu, J., Lin, Y., et al. (2011). A resource of Cre driver lines for genetic targeting of GABAergic neurons in cerebral cortex. Neuron *71*, 995–1013.

Ulanovsky, N., Las, L., and Nelken, I. (2003). Processing of low-probability sounds by cortical neurons. Nat. Neurosci. *6*, 391–398.

Ulanovsky, N., Las, L., Farkas, D., and Nelken, I. (2004). Multiple time scales of adaptation in auditory cortex neurons. J. Neurosci. *24*, 10440–10453.

Wang, Y., Gupta, A., Toledo-Rodriguez, M., Wu, C.Z., and Markram, H. (2002). Anatomical, physiological, molecular and circuit properties of nest basket cells in the developing somatosensory cortex. Cereb. Cortex *12*, 395–410.

Yuste, R. (2015). From the neuron doctrine to neural networks. Nat. Rev. Neurosci. *16*, 487–497.